Astron. Astrophys. 355, 651–667 (2000)

ASTRONOMY AND ASTROPHYSICS

HRI observations of PMS stars in NGC 2264

E. Flaccomio[1], **G. Micela**[2], **S. Sciortino**[2], **F. Damiani**[2], **F. Favata**[3], **F.R. Harnden Jr.**[4], **and J. Schachter**[4]

[1] Dipartimento di Scienze Fisiche ed Astronomiche – Università di Palermo, Italy
[2] Osservatorio Astronomico di Palermo G.S. Vaiana, Palazzo dei Normanni, I-90134 Palermo, Italy
[3] Astrophysics Division – Space Science Department of ESA, ESTEC, Postbus 299, 2200 AG Noordwijk, The Netherlands
[4] Harvard-Smithsonian Center for Astrophysics, 60 Garden Street, Cambridge, MA 02138, USA

Received 14 September 1999 / Accepted 16 December 1999

Abstract. We analyze six ROSAT HRI observations pointed toward the Star Forming Region (SFR) NGC 2264. Three are pointed to the southern star formation core, the other three about 20' to the north. We detect 169 X-ray sources, $\sim 95\%$ of which are likely to be Pre Main Sequence (PMS) stars, significantly enlarging the known population of the SFR in the area covered by the observations. Using published BVRI photometry we place the X-ray sources with well defined optical counterparts on the HRI diagram and estimate their masses and ages. Our comparison of the mass function and age distribution of the X-ray sources with results previously obtained for NGC 2264, demonstrates that deep X-ray observations provide, at least in this case, a very efficient method of selecting SFR members and does not introduce stronger biases than other methods.

Since the observation cover a time span of ~ 5 years, we are able to study in detail the X-ray variability of our sample of PMS stars. We find that: 1) a large fraction of our sources are variable on several time scales and 2) Classical T Tauri Systems (i.e. stars surrounded by disks) are significantly more variable than the rest of our sample, suggesting a role of accretion disks in the emission and/or in the absorption of the X-ray radiation.

Key words: stars: coronae – stars: formation – stars: luminosity function, mass function – stars: pre-main sequence – Galaxy: open clusters and associations: individual: NGC 2264 – X-rays: stars

1. Introduction

The study of the first stages in the formation of stars is one of the currently most active research fields in stellar astronomy. Although much progress has been made since the discovery of T-Tauri stars (Joy, 1942) several question still remain open. There are basically two classes of problems that need to be assessed: the detailed structure and evolution of single stars from the protostellar phase to the main sequence (MS), and the nature of the processes that determine and regulate the onset of star-formation within molecular clouds in the first place.

Send offprint requests to: E. Flaccomio
(ettoref@oapa.astropa.unipa.it)

Observations of star forming regions (SFRs) naturally play a fundamental role in these studies. On the one hand they permit the study of a large number of objects, often in a variety of evolutionary states, allowing studies on the first phases of stellar pre-main sequence (PMS) evolution. On the other, comparisons of SFRs with different characteristics in terms of age, metallicity, density, presence of massive stars, etc., can provide useful informations on the dependence of the formations process and of the following stellar evolution on these parameters. Of particular interest in this respect is, for example, the question of the universality of the initial mass function.

The first step in any study of a SFR is the identification of its members. For many years X-ray observations have been used to study SFRs, particularly to uncover the important population of weak lined T-Tauri stars (WTTS). Indeed the discovery of this class of PMS stars was first made possible by observations in X-rays (Feigelson & Kriss, 1981; Walter & Kuhi, 1981).

It is now a well established result that young stars, and PMS in particular, show enhanced X-ray emission ($\mathrm{Log(Lx)} \sim 29-32$) with respect to older stars, making X-ray observations of SFRs an effective way to distinguish likely members from field stars. This approach is a useful complement to proper motion studies that, especially for some of the farthest regions and/or at the low-mass end, have yet to reach the necessary completeness and reliability.

This is especially true for the SFR NGC 2264 (see eg. Flaccomio et al. 1999 for a summary of its principal characteristics). The proper motion study by Vasilevskis et al. (1965), limited to the brightest stars in the region ($V \lesssim 15.0$), has sometimes been considered inaccurate (see Sung et al., 1997). On the other hand, several studies based on the detection of the $\mathrm{H}\alpha$ emission line (Herbig, 1954; Sung et al., 1997; Marcy, 1989; Ogura, 1984) are not well suited to discover a large fraction of the NGC 2264 population, namely the WTTS that by definition do not show this spectral signature.

Selection through detection in X-rays is not likely to suffer from this bias because WTTS and CTTS (classical T-Tauri stars) are known to present similar level of X-ray emission (see eg. Damiani & Micela 1995 and Sect. 6). Moreover NGC 2264 seems well suited to this approach because of the optically thick cloud (situated right behind the SFR) which effectively obscures

background objects, thereby minimizing contamination from background field stars or extragalactic sources (cf. Sect. 4).

Simon et al. (1985) reported the analysis of three observations performed with the Einstein Observatory's Imaging Proportional Counter (IPC, Gorenstein at al. 1981). Due to the low sensitivity and resolution of these observations, these authors could only detect 7 bright X-ray sources, with very uncertain optical counterparts. Indeed the only instrument with sufficient spatial resolution to avoid source confusion for most of the sources we detect in our field of view is, up to now, the ROSAT HRI (Zombeck et al. 1990).

Our paper is organized as follows: in Sect. 2 we present the data and their analysis; Sect. 3 deals with the identification of our X-ray sources with optical counterparts. Sect. 4 discuss the degree of contamination of our sample of X-ray sources from field objects. In Sect. 5 we present the HR diagram for our X-ray sources, we discuss their mass and age distributions and we draw conclusions on the representativeness of our sample respect to the whole NGC 2264 population. Sect. 6 focus on the X-ray luminosities inferred for our sources from our observations. In Sect. 7 we present a detailed study of X-ray variability. In Sect. 8 we describe some peculiar X-ray source in our sample; finally we briefly discuss our result in Sect. 9.

2. X-ray observations and data analysis

Table 1 summarizes the HRI observations we have analyzed. The first column contains a reference number that will be used in this paper; we then report the Rosat Observation Request (ROR) number, the exposure time, the time period during which each observation was performed, the name and pointing of each field.

The first three observations (target: "North") were retrieved from the public archive and are nominally pointed toward RA 6:41:02.4, DEC 9:40:48 (J2000). These observations cover a good fraction of the Star Forming Region, including both the North and South star formation cores and achieve maximum sensitivity in the region between them. The last three observations (target: "South") were targeted by us and, while largely overlapping with the previous pointings, focus on the southern star formation core. Their nominal pointing is RA 6:41:07, DEC 9:26:24 (J2000). In the following we will refer to the two distinct pointings as the North and South pointings, respectively.

The observations span a time period of about 5 years; the total observing time varies from ~ 25 ksec. in the southernmost region to ~ 58 ksec. in the region of the overlap between the two distinct pointings.

Since the fields comprising the North and the South pointings have the same nominal coordinates, we considered adding the co-pointed images together in order to increase the sensitivity. The HRI is known to have an imperfect aspect solution (David et al. 1997), leading to discrepancies between the nominal and actual pointing of the order of several arcsecond. This problem can lead to a degraded image quality when combining several exposures without any corrections. We estimated the amount of this effect by comparing positions of detected sources with the well known positions of their optical counterparts. For this purpose we used only the most significant detections and excluded those sources with uncertain or multiple counterparts.

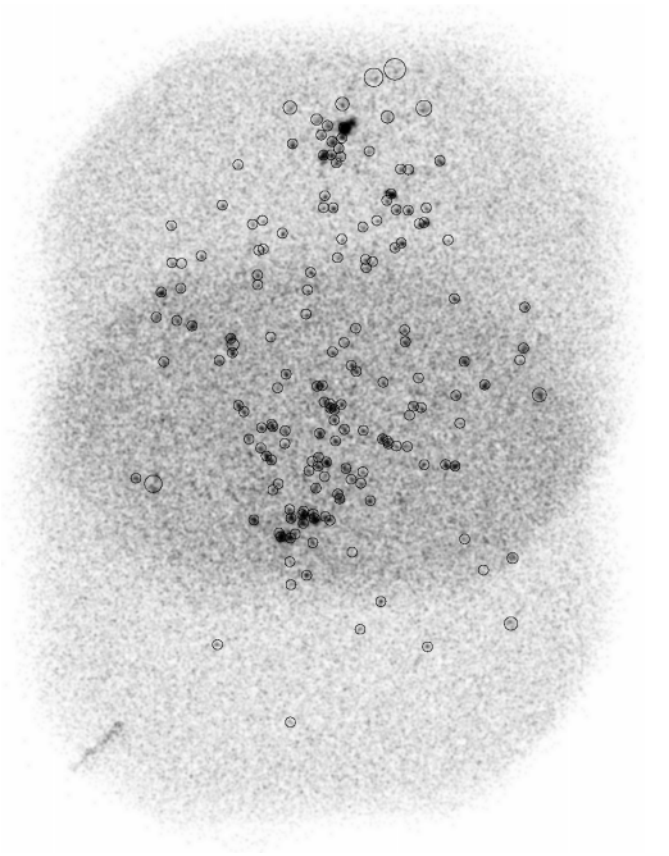

Fig. 1. Sum of the HRI exposures (cf. Table 1). The data have been smoothed with a Gaussian filter ($\sigma = 10$"); sources detected using a wavelet transform algorithm (Damiani et al. 1997a,b) are denoted with circles whose radii contain 85% of the point spread function at the given off-axis angle (from 8" at $\theta_{off} = 0'$ to 29" at $\theta_{off} = 15'$). For clarity of representation, identification radii, when smaller than 15" have been enlarged to that size.

The South pointings, all observed during Spring, were found to have small (with respect to the HRI spatial resolution) shifts, with a maximum offset between pointings of $< 3''$, while the North fields, obtained during both Spring and Fall, showed relative shifts of more than $5''$. This finding agrees with the trend sometimes observed for multiple ROSAT pointings and believed to be due to the vagaries of star tracker acquisition. For the South pointings we decided to add the three images without corrections, while for the three North images we applied the computed shifts before adding them together.

Fig. 1 shows the sum of six HRI exposures, smoothed with a $\sigma = 10''$ Gaussian filter.

2.1. Source detection

We analyzed the data using a source detection algorithm based on wavelet transforms (Damiani et al. 1997a,b) tuned for the HRI specific characteristics (see Micela et al. (1999) for further

Table 1. Summary of HRI observation segments.

Seg. ID	ROR	On Time [ksec]	Start of accepted data	Obs. Span [days]	Target field	RA_{2000} [h:m:s]	DEC_{2000} [^{o}:':"]
1	rh200130a00	19.41	1991 Mar. 20	3	North	6:41:02.4	9:40:48
2	rh200131a01	2.88	1991 Oct. 01	1	"	"	"
3	rh200130a01	11.02	1992 Sep. 18	2	"	"	"
4	rh201420n00	9.84	1994 Mar. 27	9	South	6:41:07.0	9:26:24
5	rh201847n00	7.47	1995 Apr. 05	5	"	"	"
6	rh201847a01	7.60	1996 Mar. 15	1	"	"	"

Table 2. Summary of detections.

Seg. ID	1	2	3	1+2+3	4	5	6	4+5+6
Detected in segment	97	17	58	114	36	27	32	58
Detected only in segment	6	2	2	9	4	4	6	8

details). This algorithm takes into account various instrumental effects (e.g. the variations of the effective exposure time and PSF throughout the detector surface) and allows the reliable detection of faint sources. In addition to the detections themselves the wavelet analysis also yields an intensity and an estimate of the source extension. The algorithm also generates a sensitivity map that can be used to estimate upper limits for the X-ray fluxes at specified positions, at confidence level consistent with that used for detections.

In order to study source variability on time scales of one year we analyzed both the six individual observation segments and the two summed images. We employed a detection threshold of 4.5σ which, according to extensive simulations (Damiani, private communication), result in less than 1 spurious detection per field. Since we have performed wavelet detection on eight images (two of which are not statistically independent from the others) the expected number of detections due to background fluctuations ranges between six and eight.

We consolidated detections within the North and South regions, on the basis of a positional criteria, matching sources detected in the three original observations and in the summed image. In each region we removed from our final lists a couple of sources which were detected in only one of the four images and which the wavelet code indicated might be extended. These detections likely represent the "merging" of two sources which were indeed resolved in other segments. Finally we compared detections in the region in common between the North and the South pointings and again removed from the original lists those sources which appeared resolved in the other pointing.

Table 2 summarizes the number of sources detected and retained after this matching procedure was applied to each segment and to the two summed images (identified by '1+2+3' and '4+5+6'). The same table also shows the number of detections that were found exclusively in a given image. As expected the images in which the largest number of sources was detected are the summed ones, but a number of sources also appear in only one of the original segments, likely indicating the presence of widespread variability (cf. Sect. 7)

All in all we found 169 distinct sources, detected in at least one of the images. Table 3 shows our list of sources. The columns indicate, in order: a sequential reference number, J2000 coordinates (the mean of detection positions), maximum and minimum count rates (with associated statistical uncertainties), a maximum likelihood X-ray luminosity (see Sect. 6), the significance of source detection, the probability of each source being variable (see Sect. 7), and suggested optical counterparts (cf. Sect. 3). In cases for which an upper limit falls below the detection(s), the minimum count rate is reported as an upper limit.

3. Identifications

In considering possible counterparts for our X-ray sources we examined all stars lying within a circle containing 85% of the photons from point-like detections at the given off-axis angle (from 8" on axis to about 29" at $\theta_{off} = 15'$). For those cases in which the X-ray source was detected both in the North and South pointings, and thus at two different off-axis angles, we chose the smaller identification radius.

We attempted identifications using stars from the following works: Walker (1956), Vasilevskis et al. (1965), Herbig (1954), Marcy (1989), Ogura (1984), Sung et al. (1997), Flaccomio et al. (1999), Young (private communication). Finally we inspected the Digital Sky Survey (DSS) plate of the region to investigate the presence of other, uncatalogued, counterparts.

The result is shown in the last column of Table 3 where multiple counterparts are separated by commas and multiple names for the same stars are given in parentheses. Identification names are formed by the initial of the first author of the articles cited above plus the identification number used in those papers, the only exception being the stars from the list of Young which are identified by 'MX'. The note "m" after the star name indicates that the these stars are likely NGC 2264 members according to the paper the name refers to: in the case of the proper motion study (Vasilevskis et al. 1965) this reduces to stars with membership probability greater than 50%; all the stars with strong H_α emission listed by Herbig (1954), Marcy (1989), Ogura (1984),

Sung et al. (1997) are also considered as likely members as well as those selected by Flaccomio et al. (1999) on the basis of photometry.

Of our 169 sources, 133 have single well-defined counterparts. These sources are denoted in Table 3 with an asterisk after the serial number. Out of the remaining 36 sources, 30 have multiple counterparts, either catalogued or visible in the DSS plate, while 6 have no optical counterpart at all; being in general low SNR detections, these 6 X-ray sources may be either associated with embedded sources or spurious detections (but see Sect. 8). Appendix A shows finding-charts for these latter 6 sources and for the 10 sources that are not associated with any catalogue counterpart. 80 X-ray sources are associated with at least one previously selected member of the association. The remaining 89 sources are thus associated with at least as many new candidate members.

Table 4 shows our estimates for the physical parameters of the X-ray sources which could be identified with a single optical counterparts. The columns provide: sequence number of the source, its V magnitude, B-V and $V - I_c$ colors, spectral type from Young (private communication), effective temperature, bolometric luminosity and references for the reported photometry ("F" for Flaccomio et. al., 1999; "S" for Sung et al, 1997). In some cases photometric data and spectral types have been collected from other sources, as noted at the bottom of the table.

In assigning B, V and I_c magnitudes to X-ray sources detected with unique counterpart, whenever they were available we used the values given by Flaccomio et al. (1999), while for the remaining stars we used photometry from Sung et al. (1997) who note that their I_c magnitudes are systematically smaller than those obtained by Pérez et al. (1987) by about 0.045 mag. Noting a similar offset from the Flaccomio et al. (1999) photometry, we have increased the Sung et al. (1997) I_c magnitudes by 0.045 mag.

When possible we also assign a spectral type to our sources using the list of Young (private communication) and, in a few cases as noted in Table 4, other catalogs from the literature.

4. Contamination from field X-ray sources

In order to estimate the contamination of our X-ray source sample by field objects, we computed the expected number of sources not associated with NGC 2264. Such an estimate is possible if the surface density of X-ray sources with fluxes greater than the detection threshold is known for the direction of the field of view.

NGC 2264 lies close to the galactic plane and only $\sim 20^o$ off the direction of the galactic anticenter ($b \sim 2.2^o$, $l \sim 203^o$). In this region the results of several X-ray Galactic Plane Surveys (GPS) hold. Motch et al. (1997) estimated the Log(N) vs. Log(S) relation (i.e. the surface density "N" of sources detected above a certain limiting sensitivity "S") using the ROSAT All Sky Survey (RASS) data. Because the RASS limiting flux is much less than the limiting sensitivity of our observations, this work is of limited use in our case. More useful are the results of a

Table 4. Counterparts of uinquely identified X-ray sources

N_X	V [mag.]	B-V [mag.]	V-I [mag.]	Sp. Type	$\mathrm{Log}(T_{\mathrm{eff}})$ [^{o}K]	$\mathrm{Log}(L_{\mathrm{bol}})$ [$L_\odot$]	Ref.
3	14.97	1.21	1.38		3.64	-0.00	S
4	16.40	1.55	1.82		3.59	-0.37	S
5	13.01[1]	0.92[1]					
7	13.35	0.83	0.94	K1	3.72	0.48	S
10	15.08	1.44	1.81	M1 V	3.59	0.15	S
12	15.91	1.41	1.80	M1 V	3.59	-0.18	F
14	15.44	1.29	1.48	K7 V	3.63	-0.14	S
15	15.32	1.23	1.39	K4 V	3.64	-0.14	S
16	15.16	1.29	1.59	K7 V	3.61	0.02	F
17	15.70	1.40	1.79	K7 V	3.60	-0.11	S
18	15.89	1.28	1.74		3.60	-0.21	F
19	15.74	1.30	1.56	K4 V	3.62	-0.23	S
20	17.41	1.56	2.36		3.55	-0.51	F
23	16.50	1.02	2.07	M3 V	3.57	-0.29	F
24	8.42	-0.12	-0.14	B4	4.22	2.53	S
25				M3 V			
26	14.40	1.07	1.21	K4 V	3.67	0.16	F
29	15.62	1.25	1.56	K4 V	3.62	-0.18	S
30	15.22	1.10	1.19	K4	3.67	-0.18	S
31	7.77	-0.20	0.00	B2 V[2]	4.42	2.71	S
32	15.62	1.09	1.51	K4 V	3.62	-0.20	S
33	9.04	-0.09	-0.05	B1	4.17	2.23	S
34	15.14	1.25	1.47	K4 V	3.63	-0.03	S
35	15.32	1.32	1.62		3.61	-0.04	S
36	18.51	0.61	2.75		3.52	-0.74	F
37	14.98	1.30	1.59		3.61	0.08	S
38	16.15	1.39	1.78	K7 V	3.60	-0.29	S
39	11.76	0.87	0.94	K1	3.72	1.12	S
40	17.67	2.13	2.00	M1 V	3.57	-0.79	F
41	16.38	1.08	1.89	M1 V	3.59	-0.33	F
42	15.71	1.42	2.04		3.57	0.01	S
44	16.30	1.62	1.95	M3 V	3.58	-0.27	F
45	17.01	1.42	1.76	K7 V	3.60	-0.64	F
46	10.16	0.03	0.01		3.99	1.76	F
47	16.76	1.67	2.95	M5 V	3.51	0.06	S
49	12.02	0.59	0.67	F8 V	3.80	0.95	S
50	16.05	1.12	1.60	K4 V	3.61	-0.33	F
52	16.74	1.46	2.18		3.56	-0.33	S
53	15.34	1.18	1.59	K4? V?	3.61	-0.06	S
54	14.56	0.99	1.16	K1 V	3.67	0.08	F
55	11.67	0.51	0.56	F6 V?	3.83	1.08	F
57	17.16	1.46	1.95		3.58	-0.61	F
58	11.81	0.54	0.61	F8 V	3.82	1.03	F
59	15.62	1.30	1.69		3.60	-0.12	S
62	14.91	1.11	1.58	M1 V	3.61	0.11	S
63	15.90	1.28	2.30	M3 V	3.55	0.07	F
65	10.21	-0.07	0.00	B8	4.13	1.74	F
66				M1 V			
67	4.66[2]	-0.25[2]	-0.22[3]	O7 V[2]	4.53	4.09	
68	12.51	0.94	1.02		3.70	0.85	S
69	15.42	0.00	1.53		3.62	-0.11	S
70	16.15	1.25	1.94		3.58	-0.21	S
71	15.34	1.66	2.03	K4	3.57	0.16	F
72	16.90	1.36	2.13	M1 V	3.56	-0.42	S
73	15.76	1.42	1.45	K7 V	3.63	-0.29	F
74	9.92	-0.07	-0.05	B7	4.13	1.88	S
75	14.81	1.24	1.33	K4 V	3.65	0.04	F
76	15.16	1.10	1.34	K4 V	3.65	-0.10	S
77	14.64	1.12	1.41	K1	3.64	0.15	S
78	13.44	1.30	1.44	K1	3.63	0.64	F
80	14.58	1.18	1.30	G9 V?	3.65	0.12	F
82	14.84	1.13	1.39	K1 V	3.64	0.06	S
84	12.89	0.83	0.95	G5 V	3.71	0.67	S
85	14.06	0.95	1.03	G7	3.70	0.23	F
86	15.30	1.22	1.40		3.64	-0.12	F
87		-0.14		K1 V?			F
89	12.74	0.71	0.75	G7? V?	3.79	0.68	F
90	16.07	1.05	1.63		3.61	-0.33	F
91	15.14	1.32	1.57	K4 V	3.61	0.02	S
93	16.47	1.40	2.04		3.57	-0.29	F
94	14.71	1.12	1.22	K1 V	3.67	0.04	S
96	10.88	0.04	0.16	B8	3.94	1.42	F
98	15.08	1.13	1.48	K4 V	3.63	-0.00	F
100	15.41	1.38	1.78	M1 V	3.60	0.01	F
101	13.39	0.85	0.95	G3 V	3.71	0.47	F
103	17.67	4.81	2.50		3.54	-0.54	F
105	14.91	1.10	1.54	K4 V	3.62	0.09	F
106	15.15	1.30	1.63	K4 V	3.61	0.04	F

Table 4. (continued)

N_X	V [mag.]	B-V [mag.]	V-I [mag.]	Sp. Type	$\mathrm{Log}(T_{\mathrm{eff}})$ [°K]	$\mathrm{Log}(L_{\mathrm{bol}})$ [$L_\odot$]	Ref.
107	17.75	1.55	2.31		3.55	-0.67	F
108	13.41	0.78	0.87	G5 V	3.75	0.44	S
109	15.61	1.16	1.36	K4 V	3.64	-0.26	F
110	16.44	1.43	1.91	K7 V	3.59	-0.34	S
111	14.73	1.28	1.64	K4 V	3.61	0.21	F
112	15.07	1.16	1.18	K4 V	3.67	-0.12	S
113	7.16[2]	-0.21[2]	-0.24[2]	B1.5 V[2]	4.43	3.10	
114	14.50	1.24	1.59	K4 V	3.61	0.28	F
115		0.11		A4			F
116	15.18	1.30	1.70		3.60	0.06	F
118	11.42	0.47	0.66	F5 V	3.81	1.19	F
119				M1 g?			
123				M3?			
124	16.77	1.15	1.80	K7 V	3.59	-0.53	F
126	15.53	1.28	1.65	K4 V	3.61	-0.10	F
127	16.87	1.69	2.49	M5 V?	3.54	-0.22	F
128	13.98	0.94	1.08	K1	3.69	0.28	S
131	15.30	1.42	1.91	K1	3.59	0.11	F
132	17.60	1.38	2.49	M3 V	3.54	-0.52	F
133	15.70	1.50	2.04	M3 V	3.57	0.02	F
134	15.32	1.21	1.54		3.62	-0.07	F
135	14.91	1.07	1.35	K4	3.65	0.01	F
136	18.43	1.55	2.46	M5 V	3.54	-0.86	F
138	14.31	1.18	1.33	K4 V	3.65	0.24	F
139	14.86	1.08	1.20	K1 V	3.67	-0.03	S
140				M1 g			
141	15.23	1.20	1.56	K4 V	3.62	-0.03	F
142	17.77	1.61	2.14	M3 V?	3.56	-0.76	F
143	15.42	1.19	1.38	K4 V	3.64	-0.18	S
144	15.72	1.26	1.53	K4 V	3.62	-0.24	S
145	8.68	-0.12	0.00	B6	4.21	2.35	S
146	12.67	0.71	0.83	G5 V	3.76	0.73	F
148	16.73	1.50	2.15	M5 V	3.56	-0.34	F
150	14.37	1.01	1.13	K1	3.68	0.14	F
151	7.46	-0.17	-0.20	B2 V[2]	4.35	2.95	S
152	16.89	1.48	1.86		3.59	-0.54	S
153	13.94	0.93	1.05		3.69	0.28	S
154	13.00	0.82	0.87	G5 V	3.75	0.61	S
155	14.62	1.11	1.29		3.66	0.10	S
156	14.63	1.14	1.33		3.65	0.12	S
157	9.79	0.44	0.51		3.85	1.83	F
158	15.39	1.19	1.34		3.65	-0.19	S
159	13.67	1.00	1.10		3.68	0.41	S
161	15.09	1.22	1.47		3.63	-0.01	S
162	14.16	1.04	1.12		3.68	0.22	S
163	15.74	1.25	1.46		3.63	-0.28	S

Notes: [1] Data from Sagar & Joshi (1983). [2] Data from Pérez (1987). [3] Data from Cousin (1980).

GPS performed with deeper pointed ROSAT PSPC observations (Morley et al. 1996, Pye et al. 1997, Sciortino et al. 1998). Sciortino et al. (1998) in particular extended the analysis of the previous works by both increasing the surveyed area and refining the analysis method to take into account subtle effects (fuzzy detection threshold, finite PSF effect, etc.) thus defining the Log(N) vs. Log(S) relation down to the limiting sensitivity of 10^{-3} PSPC counts sec^{-1}.

In order to use these results for our HRI data we followed the following strategy. First, from the sensitivity maps generated by our detection code (see Sect. 2.1) we computed, for each sensitivity level, the area observed with that sensitivity (i.e. the count rate above which we expect to detect sources); this step is necessary because of the significant inhomogeneity of the HRI field of view, both in terms of effective collecting area and PSF, which together produce an highly inhomogeneous sensitivity throughout the detector. Second, we converted the Sciortino et al. (1998) Log(N) vs. Log(S) from PSPC counts sec^{-1} to HRI counts sec^{-1}. The conversion factor depends on the incident spectrum: assuming a Raymond Smith emission model with kT between 0.3 and 1.4 KeV and an absorption ($\mathrm{Log}(N_H)$) between 19.0 and 20.5 the count rate conversion factor (HRI/PSPC) ranges between 0.28 and 0.40. Finally, using the results of the previous steps we evaluated the number of field sources we expect to detect in our HRI images. Depending on the value of the conversion factor between PSPC and HRI count rates this number ranges between 8 an 13.

These values are anyway upper limits to the contamination of our sample of NGC 2264 members because they relate both to foreground and background objects. Considering the presence of the dark cloud behind NGC 2264 we expect contamination only from foreground stars. In particular, extragalactic sources, which according to Motch et al. (1997) account for about 15% of the total, are likely not to be relevant in our case, so that the number of expected field sources reduces to 7 - 11 or even smaller.

5. The HR diagram

Having established that contamination from field sources is likely to be small, we assumed our X-ray sources are all at the distance of NGC 2264 and proceeded to place the counterparts in the theoretical HR diagram.

Bolometric luminosities were calculated from the dereddened I_c magnitude applying the bolometric correction given by Bessel & Stringfellow (1993). Effective temperatures were instead derived from $(V-I_c)_o$ for stars with $(V-I_c)_o > 0.0$, and from $(B-V)_o$ for bluer stars. In the first case we employed the Schmidt-Kaler (1982) color-temperature relation adapted with the aid of the Bessel (1990) color-color relation. In the second we used the Code et al. (1976) relation. In every case we have assumed an average value for the interstellar extinction: E(B-V)=0.06 or $E(V-I_c) = 0.077$ (Pérez et al. 1987).

Fig. 2 shows the HR diagram for the X-ray sources whose photometry (V and $V-I_c$) is known, along with the D'Antona & Mazzitelli (1998) evolutionary tracks and isochrones. Masses and ages for these stars were derived from this diagram by interpolation.

5.1. Mass and age distribution

We have studied the completeness of our sample of likely NGC 2264 members. Selection of PMS stars by means of X-ray imaging can introduce biases in the resulting population of the SFR. In particular the risk is to select preferentially the more active members, thus introducing biases on the yet not well known characteristics that determine activity (i.e. mass, age, rotation, etc.).

We have compared the mass and age distribution of our sample of X-ray sources with those obtained by Flaccomio et al. (1999). That study, although restricted to a smaller area in the southern part of the SFR, achieved a fair degree of completeness by using several complementary methods for the selection of members. In particular those authors were able to

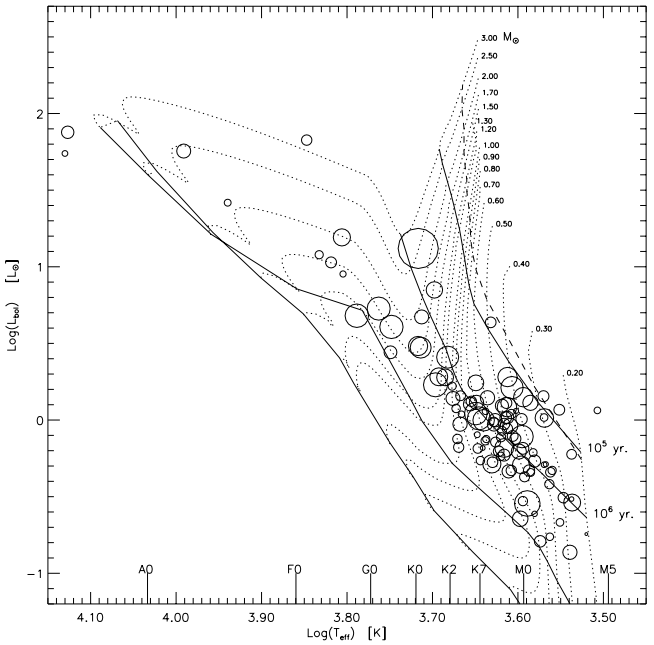

Fig. 2. HR diagram for X-ray source. The radius of circles is proportional to the logarithm of the maximum likehood count rate.

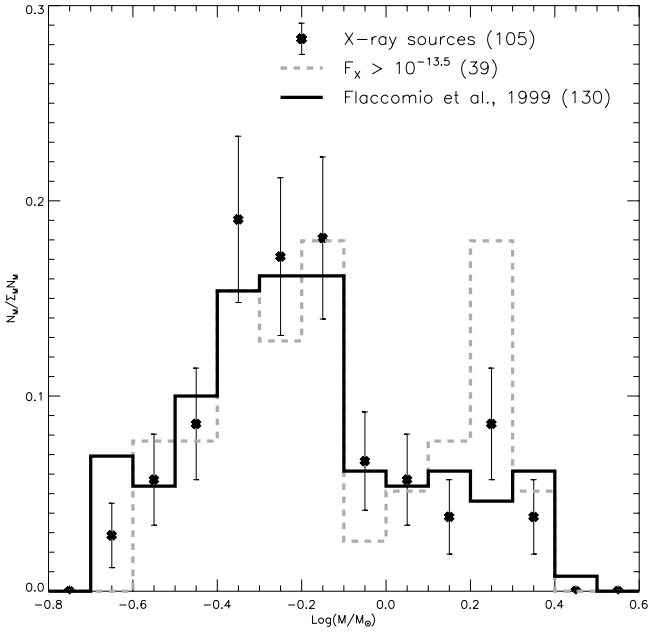

Fig. 3. Crosses: normalized mass distribution of X-ray source counterparts with error estimated from Poisson statistics (105 stars). Dotted line histogram: same distribution for stars detected with a HRI flux larger than $10^{-13.5}$ ergs cm^{-2} s^{-1} (62 stars, see text). Solid line histogram: IMF derived for the southern part of NGC 2264 by Flaccomio et al. (1999), based on 130 stars.

estimate that their composite sample was nearly complete for $\log(\mathrm{M}/\mathrm{M}_\odot) > -0.2$. Fig. 3 shows the mass distribution of our 105 X-ray sources for which we derived masses (symbols with error bars) along with the Flaccomio et al. (1999) IMF (the solid histogram). It is quite clear that the two distributions are very

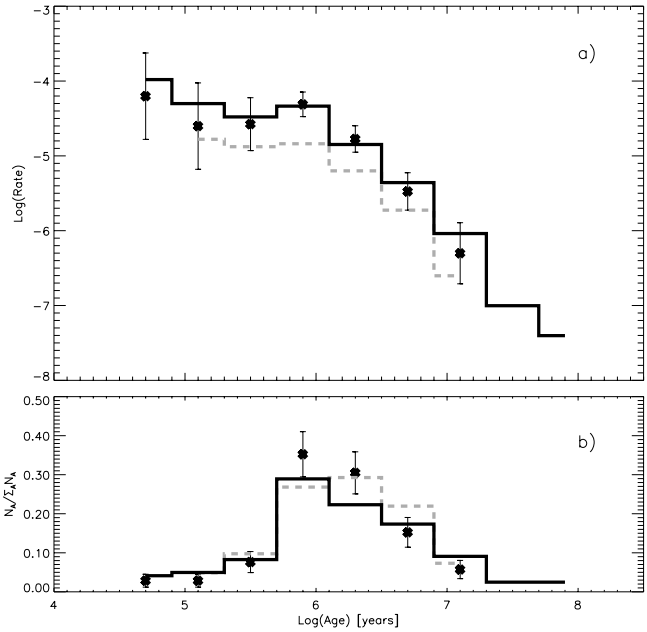

Fig. 4a and b. a Star formation rate vs. age. Crosses refer to the the X-ray selected sample studied in the present paper (105 stars); error bars are derived on the basis of Poisson statistics. The solid line histogram is the SFR derived by Flaccomio et al. (1999) for the southern part of NGC 2264 (130 stars). The dashed line refers to stars with stars detected in the X-ray with fluxes greater than $10^{-13.5}$ ergs cm^{-2} s^{-1}. **b** Normalized distribution of Log(age) for the same three samples of stars as described above

similar and that the two samples are compatible with the hypothesis that they have been drawn from the same parent population; a Wilcoxon Rank-Sum test confirm such a conclusion with high probability (P $\sim 30\%$). The same conclusion can be drawn for the Star Formation Rate and the distribution of Log(Age) which are plotted in Fig. 4a and 4b respectively.

We can then conclude that our sample of X-ray selected NGC 2264 members is as representative a subsample of the whole NGC 2264 population as was the sample studied by Flaccomio et al. (1999).

This result, i.e. that, at least for NGC 2264, X-ray selection results in a statistically representative sample of members, is naturally dependent on the limiting sensitivity of the observations. We studied this dependence by calculating mass and age distribution functions for X-ray sources detected above a given limiting flux (at the telescope) and comparing such distributions with those of Flaccomio et al. (1999). Fig. 3 and 4 show (dashed histograms) the mass function and star forming rate for a limiting flux of $3.2\,10^{-14}$ ergs s^{-1}. A Wilcoxon Rank-Sum Test shows that this mass distribution has a low ($\sim 3\%$) probability of being drawn from the same parent population as our reference sample. Decreasing the limiting flux this probability increases reaching the already mentioned value of $\sim 30\%$ for $1.0\ 10^{-14}$ ergs s^{-1}, the typical limiting sensitivity of our observations.

The previous discussion suggests that X-ray selection of star forming region members is indeed an effective tool for ob-

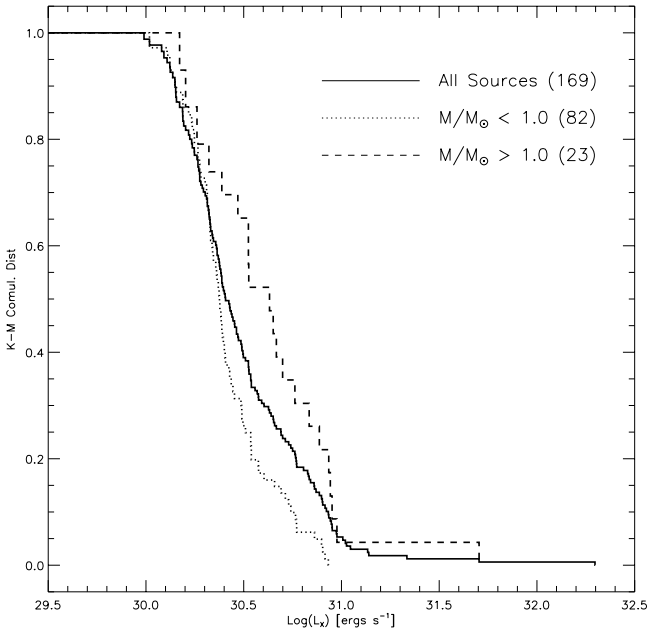

Fig. 5. Maximum likelihood X-ray luminosity distributions for the whole sample of detected sources and for two mass segregated subsamples.

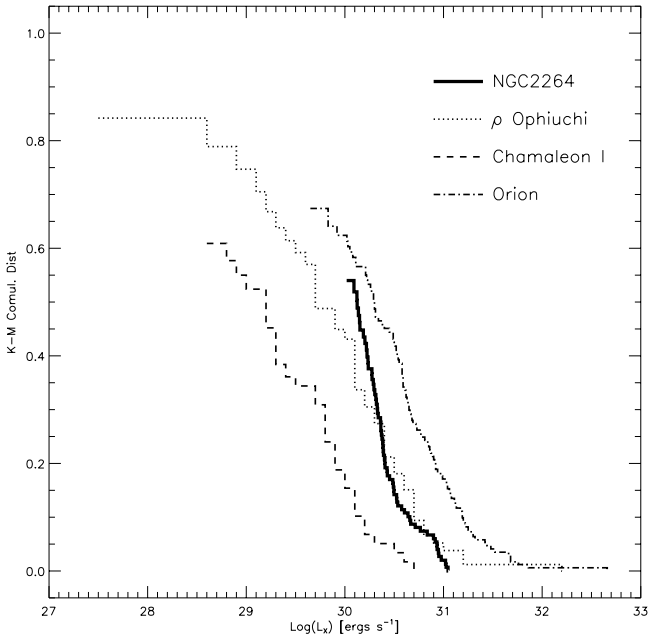

Fig. 6. Maximum likelihood X-ray luminosity function for the southern part of NGC 2264 (Flaccomio et al. 1999) and for four other SFR: ρ Ophiuchi (Casanova et al. 1995), Chamaeleon I (Feigelson et al. 1993), Orion Trapezium (Gagné et al. 1995). Note that the distribution functions are all normalized to 1 but are shown only down to the lowest detection, below of which we have no information on their shape

taining a statistically significative sample and constructing a meaningful IMF, provided that the observation have a sufficient sensitivity.

6. X-ray luminosity function

We calculated maximum likelihood X-ray luminosities under the assumption that all the detected sources were associated with the SFR (see Sect. 4) and at thus a distance of 760 pc (Sung et al. 1997).

The conversion factors between count-rate and flux in the HRI passband ($3.44\ 10^{-11}\ \mathrm{ergs\ cm^{-1}/count}$) was derived from David et al. (1997) assuming a Raymond-Smith emission spectrum with kT=0.75 keV. We calculated the interstellar absorption column density from the optical extinction ($\mathrm{A_v = R \cdot E(B-V) = 3.1 \cdot 0.06}$ mag.) using a standard ratio between $\mathrm{N_H}$ and $\mathrm{A_v}$ ($2.0\ 10^{21}$, Ryter 1996).

With two overlapping pointings, each with three different observation segments plus a combined image, observed sources could be detected (or not), in four to eight images. We first calculated, for each source, a maximum likelihood (ML) count-rate, or an upper limit to the ML count-rate, by taking into account both detections and upper limits. We used the Kaplan Meier estimator, considering all the available measurements. Because the two summed images are not statistically independent from their component segments, whenever a source was detected in one of these images we discarded the measurements from the three corresponding segments. The ML $\mathrm{L_X}$ derived from these estimates are listed in column eight of Table 3. If the lowest measurement retained in the calculation was an upper limit the computed average is treated as an upper limit.

Fig. 5 shows the ML (Kaplan Meier) distribution of these average luminosities for our entire sample of X-ray sources and for two mass-segregated groups of uniquely identified counterparts. The mean $\mathrm{Log(L_X)}$ for the entire sample is 30.49 ± 0.03 while the values for samples more and less massive than one solar mass are 30.63 ± 0.07 and 30.41 ± 0.02 respectively. There is thus an indication that the more massive stars are, on average, brighter in the X-ray band than the less massive ones. Two-population tests (in the ASURV package; Feigelson & Nelson 1995), indeed confirm this finding with good confidence ($\mathrm{P} \sim 0.2 - 0.6\%$). We also compared X-ray luminosity distributions of two other pairs of source samples: the first pair differing in their ages, the second, in the class of their optical counterparts (CTTS and WTTS according to emission in the H_α line). In both cases we found indistinguishable distributions, with probabilities of the two subsamples being drawn from the same parent population close to 50%. We conclude that X-ray luminosity does not depend on these two factors and thus that X-ray selection does not likely introduce biases on the age or on the fractions of CTTS vs. WTTS.

With the aim of obtaining an unbiased ML distribution we also calculated the X-ray luminosity function (XLF) for the southern part of the SFR studied by Flaccomio et al. (1999). We considered the ML luminosities for 77 X-ray sources falling in their surveyed area and upper limits for 73 other NGC 2264 members selected using proper motions, H_α data and BVRI photometry but not detected in the present X-ray survey. The result is shown in Fig. 6, along with similar results obtained

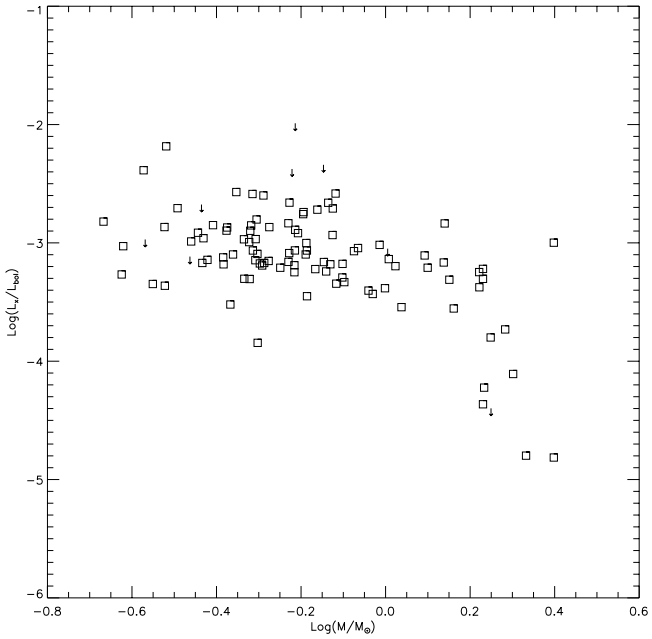

Fig. 7. $\mathrm{L_X/L_{bol}}$ vs. stellar mass. X-ray luminosities and upper limits used to compute $\mathrm{L_X/L_{bol}}$ are derived from maximum likehood count rates as described in the text.

from published data for other SFRs of different ages. The data for ρ Ophiuchi was taken from Table 2 of Casanova et al. (1995); those for the Chamaleon I region from Table 6 of Feigelson et al. (1993); those for Orion form Table 6 of Gagné et al. (1995). In all of these three cases the XLFs are computed using both detections and upper limits for variously selected samples of confirmed members of the SFRs. As these samples are not homogenous with respect to each other and to our sample (reaching, for example, different limiting masses) the four luminosity functions in Fig. 6 are not strictly comparable, especially in the light of a possible mass - $\mathrm{L_X}$ relation.

As pointed out in Sect. 5.1, our sample is likely representative of the whole population in terms of mass and age. It is apparent from the NGC 2264 XLF in Fig. 6 that we could only define about 55% of the XLF, the remaining members being fainter than our detection limit. These two seemingly contrasting indications may be explained with the absence of strong correlations between X-ray luminosities and the age and mass of PMS stars. The dependence of X-ray luminosity on mass reported above is apparently not strong enough to significantly bias our sample toward massive stars, although such an effect would clearly show up with shallower X-ray observations (cf. the dashed line of Fig. 3).

Fig. 7 shows the coronal activity indicator $\mathrm{L_X/L_{bol}}$ as a function of stellar mass. We witness the same behavior often reported for PMS stars (see eg. Alcalá et al. 1997) that can be interpreted in terms of saturation of activity at a level of $\mathrm{L_X/L_{bol}} \sim -3$ for stars less massive than ~ 1 solar mass and a decrease of this parameter for more massive stars.

7. Variability

PMS stars are known to be strongly variable sources at virtually all wavelengths, including the X-ray passband which reveals very large variations in luminosity on several time scales, ranging from hours to years (see eg. Montmerle et al. 1983). That this is the case also for our sources in NGC 2264 is made quite clear by the large number of sources we detect in only one of the analyzed observational segments. In order to give a more quantitative characterization of the variability of our sample and to relate variability to the physical characteristics of our X-ray sources, we have employed two complementary methods.

First, we have searched for the presence of variability in each of our sources using the Kolmogorov-Smirnov (KS) and the Cramer-vonMises (CvM) tests. Second, using the "variability distributions" described below, we have been able to study the variability properties of entire source subsamples.

7.1. Individual source variability

The KS and CvM tests, as implemented in the IRAF/PROS task "vartst", have been performed for each of the sources detected in the two distinct pointings (North and South). Photons were extracted from source-centered circular regions containing 85% of the Point Spread Function at the relevant off-axis. No correction for variable background emission has been applied. Both tests give as a result the confidence ($\mathrm{P_{var}}$) with which we can reject the null hypothesis that sources are indeed constant at the 90%, 95% or 99% level. Hereafter, for simplicity, we will refer to these confidence levels as "variability" probabilities, with $\mathrm{P_{var}} \leq 90\%$ indicating likely "constant" sources and $\mathrm{P_{var}} > 99\%$ likely "variable" ones. Noting that the results of the two tests are largely consistent, we report the maximum of the two variability probabilities obtained for each star in the eighth column of Table 3. Variability is detected with 95% confidence (or higher) for 52 of our sources (31% of the total). Raising the significance criterion to 99% reduces this number to 31 (18%).

These fractions however are certainly lower limits to the incidence of variability in our X-ray sources for two simple reasons. First, because of the flare-like nature of variability of some stars (see the light curves discusse in Sect. 7.4) and the limited time span of our observations, we may have observed most sources only in their quiescent state. Second, the low photon statistics of most of our sources means that the KS and CvM tests can only detect very large emission variations in those sources. We indeed have verified that the sources detected as variable are, on average, significantly brighter in the X-rays than the sources not detected as such. Although in principle this could be a real trend, it more likely reflects the difficulty of detecting variations in low intensity sources. If we restrict our analysis to sources detected above a certain count rate threshold, (see Table 5), we see that, as it increases, the luminosity distributions of sources detected and those not detected as variable ($\mathrm{P_{var}} < 90\%$ and $\mathrm{P_{var}} \geq 90\%$) become statistically indistinguishable as indicated by the KS test probabilities that the two

Table 5. Summary of variability analysis.

Threshold (10^{-3}cnt s^{-1})	0.0	2.0	2.5
N_{tot}	169	44	**32**
$N[\geq 90\%]$	65	24	16
$N[\geq 99\%]$	31	16	**12**
$P^{KS}_{C-rate}[90\%]$	4%	65%	71%
$< Log[Age_{\geq 90\%}] >$	6.1 ± 0.1	6.0 ± 0.1	6.0 ± 0.2
$< Log[Age_{<90\%}] >$	6.1 ± 0.1	6.4 ± 0.2	6.8 ± 0.1
$P^{KS}_{Age}[90\%]$	60%	4%	2%
$N_{H\alpha}$	31	6	5
$N_{H\alpha}[\geq 90\%]$	13	6	5
$N_{H\alpha}[\geq 99\%]$	7	5	**5**

samples are drawn from the same parent population(P^{KS}_{C-rate} in Table 5).

Moreover, as can be seen from N_{tot}, $N[\geq 90\%]$ and $N[\geq 99\%]$ in Table 5, the fraction of variable sources increases significantly increasing the luminosity threshold. In the following analysis we will thus consider, not only the entire sample, but also subsamples of bright sources that can be more reliably distinguished as variable or non variable.

7.2. Derivation of variability distributions

The other method we employed is similar to that described in Montmerle et al. (1983), Sciortino & Micela (1992), Schmitt et al. (1993) and Marino et al. (1999). It compares the different count rates, or count rate upper limits, measured in each of our 6 observational segments for each source. Given the time lapse between these segments this method is more likely to detect variability on long time scales ($\sim$ 1 year). For each X-ray source of the sample under study we have calculated the minimum of the available independent measurements (either three or six) and the ratio between the remaining measurements and this minimum. Whenever the numerator of this fraction was an upper limit we also considered the calculated fraction as such. We then constructed the Maximum Likelihood (Kaplan-Mayer) distribution of all these ratios (we will call it the "observed" distribution) and compared it to the distribution we would obtain if all sources were constant and differences were due only to counting statistics. Before explaining how we obtained this latter ("constant") distribution, we note that, due to the way we have treated upper limits, the "observed" distribution is actually narrower than it should be and thus gives a conservative estimate of variability. This is because, when the minimum measurement is an upper limit, we consider it, for the sake of this calculation, as a detection. It follows that, if the numerator of the ratio is a detection, the calculated value will be smaller than the real one. If, on the other hand, the numerator is itself an upper limit the ratio will also be considered an upper limit, although the actual value might as well be larger.

The "constant" distribution is calculated by simulating the observation and the measurement of the X-ray flux of our 169 sources, considered constant and with count rates equal to the minimum of the our measures. For the simulations we assume

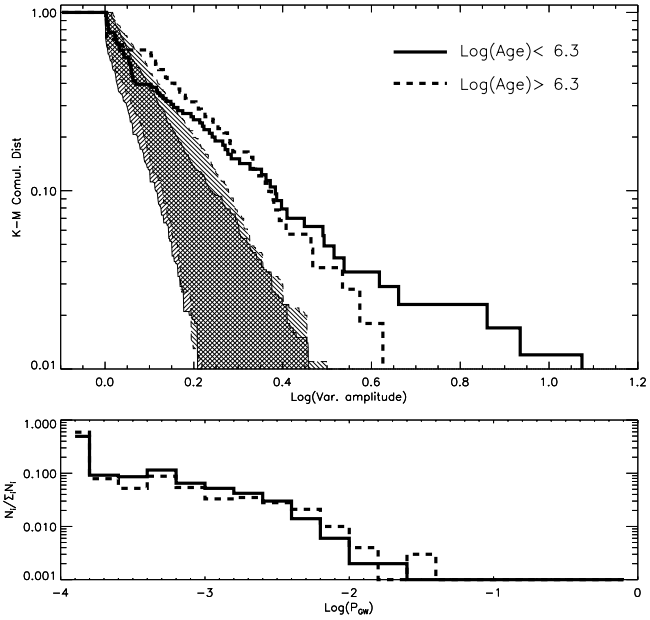

Fig. 8. Upper panel: maximum likelihood distributions (see text) of count-rate ratios between different measurements of the same source at different times. The solid and dashed lines refer to stars younger and older than $10^{6.3}$ years. The overlapping shadowed areas refer to the 0.5% and 99.5% quantiles of the simulated "constant" distributions (see text); the bounding lines are of the same style of the "observed" distribution they refer to. Lower panel: distributions of the probability (P_{GW}) that the "observed" curves are compatible with each of the 1000 simulated "constant" distributions. Line styles have the same meaning as in the upper panel.

Poisson statistics. Moreover, in order to simulate the detection or the non-detection of our simulated sources, we use the sensitivity maps generated by the wavelet detection code (Damiani et al. 1997a) for our HRI sequences. Once the detection (or non detection) and photometry of our constant sources has been simulated we calculate the ML ratio distribution using the same procedure used for the "observed" distribution. Through this simulation process we calculated 1000 distributions. To evaluate the compatibility of these simulated distributions with the "observed" ones we followed two strategies: first, we established, for each bin, the 0.5% and 99.5% quantiles of the 1000 distributions; second, for each simulation we ran a Gehan's generalized Wilcoxon test (using hypergeometric variance) and recorded the probability (P_{GW}) that the simulated distribution of ratios is compatible with the observed one. The result is that shown in Figs. 8 and 9, where, in the upper panel the thick lines represent the "observed" distributions and the hatched areas the confidence intervals of the "constant" ones just described. In the lower panels we show the distribution of P_{GW}.

7.3. Variability and stellar parameters

We also examined the dependence of variability on several stellar parameters. For this purpose we considered only sources with unique optical counterparts and with estimated physical

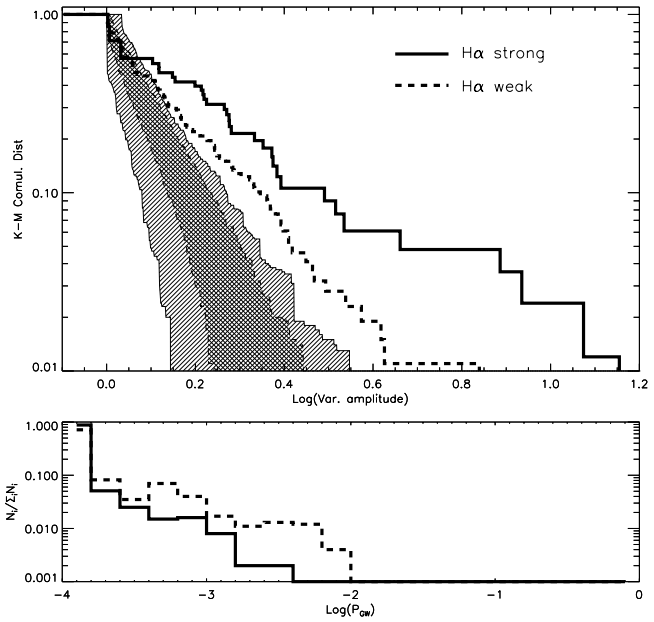

Fig. 9. Same as Fig. 8 but for subsamples whose (unique) counterparts are cited in the literature as having strong or weak H_α emission.

characteristics. We compared masses, ages, bolometric luminosities, H_α emission, etc. of subsamples of variable and non variable X-ray sources (according to the above tests). Moreover, we compared the luminosity-ratio distributions of subsamples of different mass, age, etc.

In most cases, variable and constant sources did not show significant differences, indicating that the parameters in question do not play an important role in the X-ray emission and/or its variability in time. There were, however, two notable exceptions: age and H_α emission.

Table 5 shows the mean $\mathrm{Log(Age)}$ of the variable and non variable sources (the labels "$\geq 90\%$" and "$< 90\%$" refer to $P_{\rm var}$) as well as the probability, $P^{\rm KS}_{\rm Age}$, that the two age samples have been drawn from the same parent population according to the KS test. It can be seen that for the lowest value of count rate threshold, the two samples are indistinguishable. If we consider only the brightest sources (whose $P_{\rm var}$ is more meaningful) the variable stars appear to be significantly younger than the non variable ones. This indication is only partially supported by Fig. 8, which shows the distributions of luminosity ratios for stars older and younger than $10^{6.3}$ years. Both samples appear to be composed of variable stars, but the difference between the older and the younger stars is not very striking, apart from the presence of a tail of high amplitude variability in the younger sample.

A more striking discriminant of X-ray variability is the presence or absence of strong H_α emission. Because we collected H_α information for our stars from several sources in the literature, we lack a consistent basis for comparing the strength of the line. We have therefore classified the stars qualitatively as being either emitters or non-emitters of H_α flux. The incidence of variability in the emitters is much higher than among those characterized as non H_α emitters. This can be seen by considering the bold-text numbers in the right-most column of the table (i.e., those above the $2.5\ 10^{-3}\mathrm{cnt\ s^{-1}}$ threshold). For this 32-source sample, all of the H_α emitters (5 out of 5) are variable, as compared to only about a quarter (12-5=7 out of 32-5=27) of the non-emitters. We recall (see Sect. 6) that no difference was found in the X-ray luminosities of stars with and without strong H_α emission, implying that this result cannot be explained in terms of selection effects due to counting statistics. This same conclusion regarding the variability of the two samples of PMS stars with and without strong H_α emission can be independently drawn from Fig. 9: although both samples are variable, the X-ray emitting stars with strong H_α emission are significantly more variable in X-rays than those with weak H_α emission.

7.4. Light curves and flares

In order to visually verify the result of the variability tests and to gain insight into the nature of this variability, we plotted light curves for each of our sources. Figs. 10 and 11 show these curves for sources with strong evidence of variability. These light curves, as well as others which are not shown, can be roughly divided in two groups: those that indicate variability on long ($\sim$ 1 year) time scales (eg. X-10, X-135) and those that show short-lived flares (eg. X-159, X-85, X-125).

Our HRI observations are heavily fragmented in time. It is thus not easy to observe a flare in its entirety. Fig. 12 shows a strong flare that occurred on a G5 V star (source X-85) on September 19 1992, toward the end of the third observation segment of Fig. 10. Although, due to the low statistic and the limited time coverage of the observations, few conclusions can be drawn on the real shape of the light curve, it seems likely that the flare began at the end of the first observation segment shown in Fig. 12 and that the emission peak occurred during the data gap between the two segments, and was not observed. In any case we do observe a $\sim$26-fold increase in the X-ray emission from this star, from a mean level of $\sim 1.4\ \mathrm{Counts\ ksec^{-1}}$ observed in the rest of the observing time to about 37 $\mathrm{Counts\ ksec^{-1}}$. Even assuming we have seen the peak, X-85 became the second brightest X-ray source in the region (after S Mon, our source X-67) during this flare. If we assume the same count-rate to flux conversion factor as derived in Sect. 6 the inferred peak luminosity is $\sim 8.7 \times 10^{31}\ \mathrm{ergs\ s^{-1}}$, while the total energy release during the 50 minutes in which the emission is seen to decay, i.e. the second observation segment in Fig. 12, is about 1.9×10^{35} ergs. This last value is certainly a lower limit to the total energy emitted during the flare, as it includes neither the tail, nor the rise (and probably the peak) of the flare. Although considerably fainter than flares reported by Preibisch et al. (1993) on $\mathrm{LkH}\alpha$ 92 (IC 348), and by Preibisch et al. (1995) on P1724 (Orion) this flare is nevertheless among the most powerful events observed from T Tauri stars, comparable to that observed by Montmerle et al. (1983) on ROX 20 in the ρ Ophiuchi region.

Another powerful X-ray flare in an NGC 2264 member is observed in the Einstein IPC data whose analysis is reported in Simon et al. (1985). Their source 4 likely undergoes a flare during their third observation (reported $L_X \sim 3.1\ 10^{31}$), the

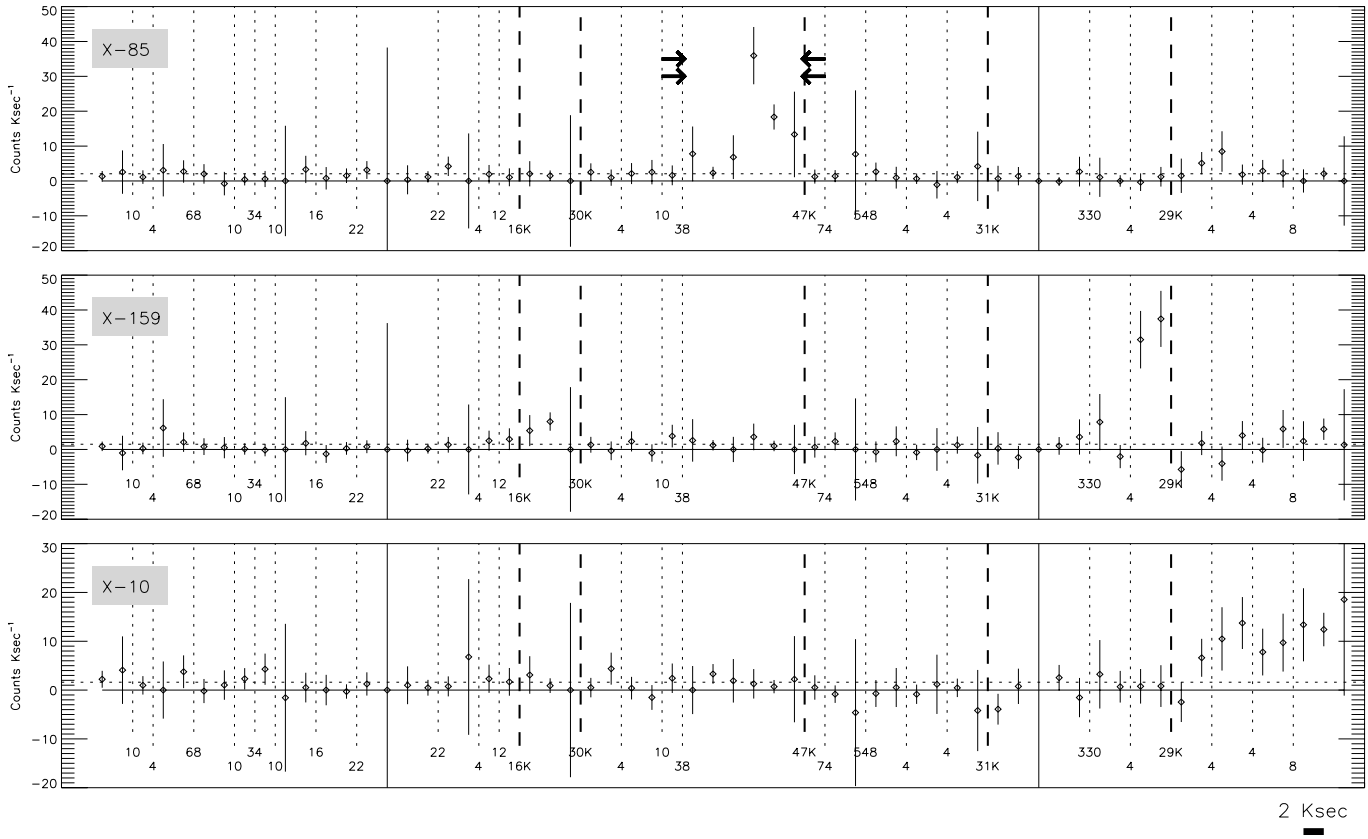

Fig. 10. Light curves for three X-ray sources with clear evidence for variability. For each source, background subtracted count-rates, binned in 2000 seconds intervals, are shown as function of time along with error bars (solid vertical lines) derived from counting statistics. Gaps have been suppressed in the time axis; between gaps the scale is as indicated by the 2 ksec bar at the bottom right. The source sequence number is indicated in the upper left corner of each plot. Vertical lines represent gaps in the observation between adjacent bins: thin dotted lines represent gaps larger than $2 \cdot 10^3$ sec., while thick dashed lines separate the different observations. The number at the bottom of the line gives the width of the gap in units of 10^3 and 10^6 seconds, for the dotted and dashed lines, respectively. The dotted horizontal lines indicates the average count-rate as derived from the light curve. The arrows in the top panel (source X-85) indicate the part of the light curve which is shown in more detail in Fig. 12.

only one in which it is clearly visible. We do not detect any HRI X-ray source within the IPC error circle for this source and estimate an upper limit on its luminosity of $5.2\ 10^{30}$ ergs s^{-1}, a factor of at least 6 less than the Simon et al. (1985) value.

It is quite likely that these are not isolated cases. Several other sources show signs of sudden brightening at about the same level, but, as already pointed out, their low statistic and the poor sampling of the light curves does not permit further study. The long uninterrupted observations with CHANDRA and/or XMM will give us the opportunity to shed further light on this subject.

8. Comments on individual sources

X-27: This HRI source has no visible counterpart either catalogued or in the DSS plate (see Appendix). It lies within the area surveyed by Flaccomio et al. (1999) with CCD photometry. We looked for counterparts in the CCD frames analized in that work and we found a faint counterpart in the I band frame close to the center of our identification circle. It is likely to be a very reddened, embedded, source.

X-39: The second brightest X-ray source in our list. This source is identified with the W UMa system W92. Simon et al. (1985), observing this source with the Einstein IPC (their source 4), were not able to identify it unambiguously because of the low resolution of their observations. Assuming the distance of NGC 2264 they estimated an $\mathrm{Log}(\mathrm{L_X}) \sim 31.4$ lower than our luminosity ($\mathrm{Log}(\mathrm{L_X}) = 31.70$) by a factor of about 2. If at the distance of NGC 2264 X-39 would be brighter in the X-rays than any of the W UMa systems studied by McGale et al. (1996) by a factor of at least 15. This star is thus likely to be a foreground object.

X-67: The brightest X-ray source in our field of view. It is associated with the O7 V star S MON. Its X-ray emission has been studied by Snow et al. (1981), who detected significant luminosity variability in three Einstein IPC observations. No evidence of variability is apparent in our data for this source. Its $\mathrm{Log}(\mathrm{L_X}/\mathrm{L_{bol}})$ is about -5.4, at the upper extreme of $\mathrm{Log}(\mathrm{L_X}/\mathrm{L_{bol}})$ ratio found by Sciortino et al. (1990).

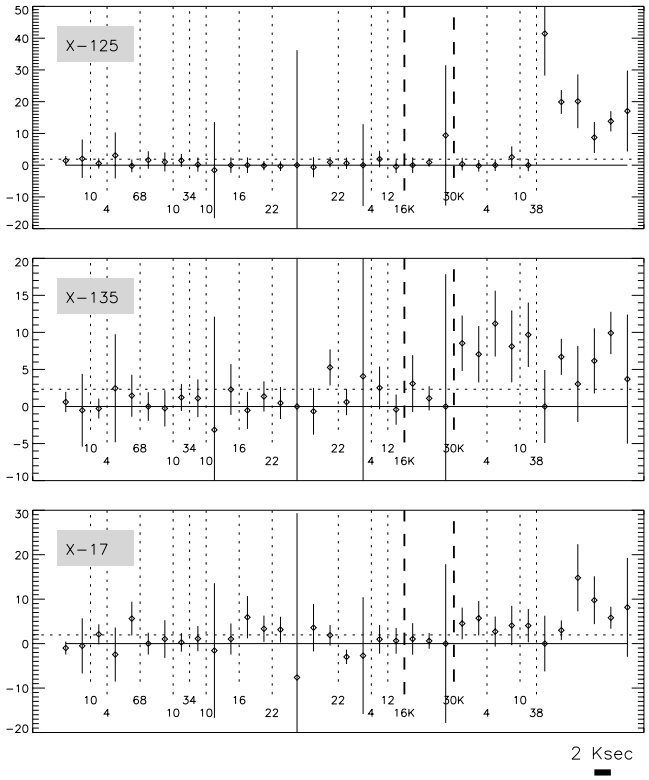

Fig. 11. Same as Fig. 10. Note that while the sources in Fig. 10 are observed in all 6 observational segments, these light curves refer only to the north field (segments 1,2 and 3).

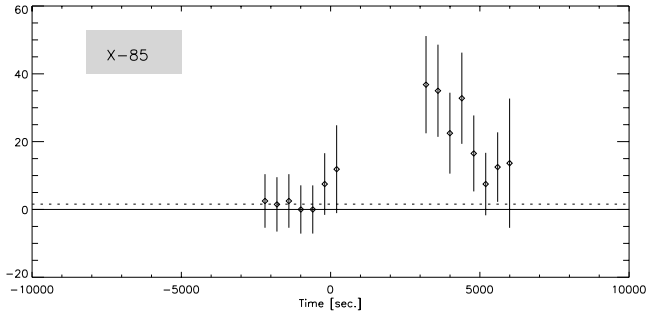

Fig. 12. Flare on the source X-85. Photons are binned in 400 seconds intervals. The dotted horizontal line indicates the average count rate computed for the rest of the light curve, i.e. excluding the interval shown here (cf. Fig. 10). Error bars are derived from counting statistics.

9. Summary and conclusions

We analyze six pointed ROSAT HRI observations of a large fraction of the Star Forming Region NGC 2264 detecting 169 X-ray sources, 133 of which can be identified with a single optical counterpart. We estimate about 5% contamination from field objects, so that almost all of our X-ray sources have as counterparts members of the SFR. We thus increase the known population of this SFR by about 90 stars. Collecting optical data from the literature, we are able to place a large fraction of the X-ray sources on the HR diagram and to estimate their masses and ages through the D'Antona & Mazzitelli (1998) evolutionary tracks. We compare masses and ages of our X-ray sources with those of the sample studied by Flaccomio et al. (1999), which, though restricted to the southern core of NGC 2264, achieved a good degree of completeness by using several complementary selection methods. We find that our X-ray sources are representative of the whole population of NGC 2264 members in terms of distributions of ages and masses and suggest that sufficiently deep X-ray observations provide one of the best methods of selecting the important population of WTTS in SFRs.

The long time span of the observations permit a study of the time variability properties of our source sample. Using different, complementary techniques, we find that variability is significantly more widespread among stars with strong H_α emission (i.e. CTTS) and also, to a lesser degree, among the youngest sources. We tend to interpret this latter result as a byproduct of the strong dependence of variability on whether the star is a CTTS or a WTTS. Indeed we have indications that, among our X-ray sources, CTTS are on average slightly younger than WTTS ($< \mathrm{Log(Age_{CTTS})} > = 5.97 \pm 0.08$, $< \mathrm{Log(Age_{WTTS})} > = 6.18 \pm 0.05$; results of the two sample tests performed by ASURV: 0.7% - 6%). We are thus induced to give a more fundamental role to the dependence of variability on the PMS class of the star. This result points to a role of the accretion process and/or of the circumstellar disk either in the X-ray emission mechanism or in its modulation. With the present data we are not able to say what the nature of this role might be: we confirm that X-ray luminosities of CTTS and WTTS are comparable, so that accretion is not likely to be responsible for a significant part of the emission. On the other hand we can envision a couple of mechanisms that might explain the influence of disks on X-ray luminosity of CTTS: one is the distortion of the coronal magnetic field due to the presence of the accretion disk, which might, for example, produce large loops that extend to the inner part of the disk or induce stresses on the magnetic field due to the accretion flow. Another is the variable extinction due to a non-homogeneous disk or wind occulting the X-ray emitting region of the star. Both these hypothesis are susceptible of verification with improved optical data and with new, deeper and spectrally resolved X-ray observations.

Acknowledgements. We thank Dr. E. Young for providing the catalog of spectral types prior to publication. EF, GM, SS, FD acknowledge partial financial support from MURST (Ministero della Università e della Ricerca Scientifica e Tecnologica) and ASI (Agenzia Spaziale Italiana). EF thanks the "Università degli Studi di Palermo" for awarding a fellowship.

Appendix A: Finding charts of unidentified sources

References

Alcalá J.M., Krautter J., Covino E., et al., 1997, A&A 319, 184
Bessel M.S., 1990, PASP 102, 1181
Bessel M.S., Stringfellow G.S., 1993, ARA&A 31, 433
Casanova S., Montmerle T., Feigelson E.D., André P., 1995, ApJ 439, 752
Code A.D., Davis J., Bless R. C., Hanbury Brown R., 1976, ApJ 203, 417

Cousin A.W.J., 1980, South African Astronomical Observatory Circular 1, 234
Damiani F., Micela G., 1995, ApJ 446, 341
Damiani F., Maggio A., Micela G., Sciortino S., 1997a, ApJ 483, 350
Damiani F., Maggio A., Micela G., Sciortino S., 1997b, ApJ 483, 370
D'Antona F., Mazzitelli I., 1998, In: Micela G., Pallavicini R., Sciortino S. (eds.) Mem. Soc. Astron. Ital. Vol. 68. No. 4
David L.P., Harnden F.R. Jr., Kearns K.E., Zombeck M.V., 1997, The ROSAT High Resolution Imager (HRI) Calibration Report
Feigelson E.D., Kriss G.A., 1981, ApJ 248, L35
Feigelson E.D., Nelson P.I., 1985, ApJ 293, 192
Feigelson E.D., Casanova S., Montmerle T., Guibert J., 1993, ApJ 416, 623
Flaccomio E., Micela G., Sciortino S., et al., 1999, A&A 345, 521
Gagné M., Caillault J.P., Stauffer J.R., 1995, ApJ 445, 280
Gorenstein P., Harnden F.R. Jr., Fabricant D.G., 1981, I.E.E.E Transactions on Nuclear Science. volume NS-28, p. 869
Herbig G., 1954, ApJ 119, 483
Joy A.H., 1942, ApJ 96, 344
Marcy G.W., 1989, AJ 85, 230
Marino A., Micela G., Peres G., 1999, A&A submitted
McGale P.A., Pye J.P., Hodgkin S.T., 1996, MNRAS 280, 627
Micela G., Sciortino S., Harnden F.R.Jr., et al., 1999, A&A 341, 751
Montmerle T., Koch-Miramond L., Falgarone E., Grindlay J.E., 1983, ApJ 269, 182
Morley J.E., Pye J.P., Warwick R.S., Pilkington J., 1996, In: Zimmermann H.U., Tr/"umper J., Yorke H. (eds.) MPE Report 263, Röntgenstrahlung from the Universe. p. 659
Motch C., Guillout P., Haberl F., et al., 1997, A&A 318, 111
Ogura K., 1984, PASJ 36, 139
Pérez M.R., Thé P.S., Westerlund B.E., 1987, PASP 99, 1050
Preibisch Th., Zinnecker H., Schmitt U.H.M.M., 1993, A&A 279, 33L
Preibisch Th., Neuhauser R., Alcalá J.M., 1995, A&A 304, 13L
Pye J., Morley J.E., Warwick R.S., et al., 1997, In: Micela G., Pallavicini R., Sciortino S. (eds.) Cool Stars in Clusters and Associations: Magnetic Activity and Age Indicators. Mem. Soc. Astron. Ital. 68, p. 1089
Ryter Ch.E., 1996, Ap&SS 236, 285
Sagar R., Joshi U.C., 1983, MNRAS 205, 747
Schmidt-Kaler T.H., 1982, In: Shaifers K.E., Voigt H.H. (eds.) Stars and Star Clusters. Landolt-Bornstein New Series, Volume 2b, Astronomy and Astrophysics, New York
Schmitt J.H.M.M., Kahabka P., Stauffer J., Piters A.J.M., 1993, A&A 277, 114
Sciortino S., Vaiana G.S., Morossi C., et al., 1990, ApJ 361, 621
Sciortino S., Micela G., 1992, ApJ 388, 595
Sciortino S., Damiani F., Favata F., Micela G., Pye J., 1998, Astron. Nachr. 319, 108
Simon T., Cash W., Snow T.P. Jr., 1985, ApJ 293, 542
Snow T.P. Jr., Cash W., Grady C.A., 1981, ApJ 19, L244
Sung H., Bessell M.S., Lee S.-W., 1997, AJ 114, 2644
Vasilevskis S., Sanders W.L., Balz A.G.A.J., 1965, AJ 70, 797
Walter F.M., Kuhi L.V., 1981, ApJ 250, 254
Walker M.F., 1956, ApJS 2, 365
Zombeck M.V., Conroy M., Harnden F.R. Jr., et al., 1990, Proceedings of the SPIE Conference on EUV, X-Ray and Gamma-Ray Instrumentation for Astronomy, 1344, 267

Table 3. List of detected X-ray sources

N_X	RA_{2000} h m s	DEC_{2000} ° ′ ″	$\mathrm{Rate_{max}}$ [c/ksec.]	err	$\mathrm{Rate_{min}}$ [c/ksec.]	err	$<\mathrm{Log(L_X)}>^{a}$ $[ergs\,s^{-1}]$	SNR	$\mathrm{P_{var}}$	Identifications
1	6 40 05.8	9 35 50.2	5.68	1.9	1.58	0.5	30.83	6.0		V20^m(S44), S42, S45, S46
2	6 40 09.7	9 41 43.8	2.60	0.7	1.68	0.4	30.77	10.6	90	V22^m(S52), S53
3*	6 40 10.1	9 38 58.9	5.17	1.0	1.13	0.4	30.86	9.2	99	S54(O66^m)
4*	6 40 11.1	9 38 11.2	0.93	0.4	0.93	0.4	30.35	4.9		S56^m(H5^m)
5*	6 40 13.1	9 24 51.2	4.83	1.4	2.25	0.8	30.84	9.1		V25^m
6*	6 40 13.5	9 20 27.2	4.75	1.6	1.81	0.7	30.97	6.8		
7*	6 40 20.6	9 36 31.2	3.06	0.8	1.98	0.6	30.76	11.9	90	W42(V29^m, S74, MX8)
8*	6 40 21.0	9 24 03.5	3.84	1.3	<1.24		<30.65	4.8	95	
9	6 40 26.0	9 26 08.5	1.27	0.6	<0.97		<30.42	4.6		
10*	6 40 26.1	9 38 04.8	10.54	1.6	1.45	0.4	30.77	12.1	99	W48(S94, MX17)
11	6 40 27.3	9 33 56.3	0.83	0.3	0.83	0.3	30.29	4.5		
12*	6 40 28.4	9 35 48.2	1.78	0.6	1.13	0.3	30.43	7.7		W51(S96, F29, MX24)
13	6 40 28.6	9 31 02.5	3.77	1.1	<0.62		30.64	12.8		V38(S98^1, S99^{1,m}, O77^m, F31)
14*	6 40 28.8	9 42 19.0	1.55	0.5	<0.92		30.34	6.9		S101(MX25)
15*	6 40 30.5	9 46 15.3	0.78	0.2	0.66	0.2	30.27	7.2		S108(O81^m, MX32)
16*	6 40 31.2	9 31 09.3	2.25	0.7	1.12	0.4	30.45	7.0	95	W56(V41, S111, O82^m, F52, MX36)
17*	6 40 32.7	9 51 35.7	6.46	1.0	2.09	0.7	30.90	11.9	99	S118(M362^m, MX40)
18*	6 40 36.1	9 18 54.1	3.10	1.1	1.58	0.5	30.57	7.2		F92^m
19*	6 40 36.4	9 48 25.3	1.29	0.4	1.15	0.3	30.44	6.3		S130(MX52)
20*	6 40 37.0	9 31 08.8	1.70	0.6	<0.99		30.37	6.4	90	F102
21	6 40 37.0	9 55 07.4	3.43	1.1	3.22	0.9	30.90	8.3		W68(V48^m, S136), S135(MX57)
22	6 40 37.0	9 47 25.9	6.58	2.2	3.48	0.6	31.13	14.2		W66(V46^m, S132, MX53), W67(V47^m, S133, MX56)
23*	6 40 37.8	9 34 59.0	0.76	0.3	0.56	0.2	30.12	5.5		S141^m(F110, MX62, H16^m)
24*	6 40 38.3	9 47 21.4	1.78	0.5	<0.72		<30.41	14.2		W74(V52, S142, MX66)
25*	6 40 38.5	9 36 59.0	0.90	0.4	<0.51		<30.18	4.6	95	MX68
26*	6 40 39.9	9 35 04.1	0.92	0.3	0.87	0.3	30.34	6.7		W77(V54^m, S150^m, F134, MX73, H18^m)
27	6 40 40.9	9 34 28.4	1.86	0.7	<0.97		<30.48	4.6	95	
28	6 40 41.2	9 50 59.1	3.22	1.0	<1.32		30.86	6.6		W78(S156^m, MX77, H20^m), S152(O87^m, MX74)
29*	6 40 41.3	9 48 14.9	3.24	0.5	1.26	0.5	30.74	11.9	99	S158(MX80)
30*	6 40 41.6	9 32 22.0	1.67	0.7	<0.72		<30.36	4.6	95	S166(MX87)
31*	6 40 42.1	9 39 24.6	7.73	2.3	1.00	0.4	30.69	10.4	95	W83(V58^m, S165^m)
32*	6 40 42.3	9 40 12.8	1.58	0.5	<0.97		30.38	6.0		S164^m(MX84, H23^m)
33*	6 40 43.1	9 46 03.4	4.88	1.9	4.25	0.7	31.01	20.6		W88(V61^m, S169, MX92)
34*	6 40 43.3	9 51 01.6	1.75	0.5	1.30	0.4	30.49	7.1	95	S170(MX91)
35*	6 40 44.5	9 48 17.4	1.89	0.5	1.59	0.3	30.58	10.2		S172
36*	6 40 44.5	9 32 24.1	0.95	0.4	<0.44		30.02	4.7		F188
37*	6 40 44.9	9 57 44.2	2.48	0.8	2.48	0.8	30.77	4.6		S175
38*	6 40 44.9	9 45 44.1	3.22	0.4	<0.93		30.69	15.0	99	S177(MX101)
39*	6 40 45.9	9 49 21.5	21.53	1.6	20.29	1.1	31.70	52.0	90	W92(V67, S181, MX106)
40*	6 40 46.6	9 32 33.6	1.17	0.6	<1.06		<30.42	4.7		F207(MX112)
41*	6 40 46.8	9 32 43.1	2.29	0.8	<1.06		30.40	6.8	99	W95(S186^m, F211^m, MX112, H26^m)
42*	6 40 46.9	9 54 31.6	2.47	0.7	2.26	0.6	30.73	7.0	99	S183
43	6 40 47.1	9 48 55.3	0.78	0.3	0.68	0.3	30.27	5.9		S184, S187
44*	6 40 48.1	9 36 41.4	2.14	0.7	0.69	0.2	30.44	6.6	95	W97(S191, F219^m, MX117)
45*	6 40 48.2	9 32 52.2	3.39	1.1	<0.65		<30.60	8.2	95	W101(S193, F221, MX121)
46*	6 40 48.7	9 21 56.3	2.69	0.8	<1.12		30.52	8.5	99	V73^m(F223)
47*	6 40 49.8	9 47 34.1	0.95	0.3	0.66	0.2	30.19	6.5	95	S198(O95^m, MX125)
48	6 40 50.6	9 57 11.6	2.24	0.7	1.89	0.6	30.65	5.2		S197
49*	6 40 50.9	9 44 47.8	2.42	1.2	<0.57		30.17	6.3		W108(V78^m, S206, MX132)
50*	6 40 51.6	9 28 43.9	1.96	0.7	<0.91		30.49	8.0		F250^m(MX134, H34^m)
51	6 40 51.8	9 52 13.9	1.16	0.4	1.16	0.4	30.44	4.8		S213(MX135), S214(MX140)
52*	6 40 52.7	9 44 24.1	0.99	0.3	0.78	0.3	30.27	7.4		S215
53*	6 40 52.9	9 44 56.6	1.48	0.5	0.90	0.3	30.36	8.6		S216^m(O98^m, MX141)
54*	6 40 53.4	9 33 26.7	0.79	0.3	0.79	0.3	30.28	5.5		W115(V82^m, S217^m, F263, MX143, H35^m)
55*	6 40 53.6	9 30 39.6	1.62	0.6	<0.49		<30.26	5.3	99	W116(V83^m, S218, F262, MX144)
56*	6 40 53.6	9 47 07.8	1.22	0.4	<1.00		30.46	5.3		
57*	6 40 54.1	9 29 53.8	0.91	0.4	0.58	0.2	30.14	5.1	95	F264
58*	6 40 54.3	9 20 04.2	1.03	0.3	<1.03		30.39	5.3		W118(F266, MX147)
59*	6 40 55.3	9 37 24.9	1.45	0.5	1.05	0.3	30.40	9.0		W119(S228)
60*	6 40 55.5	9 40 19.2	0.88	0.4	<0.41		29.99	4.7		
61	6 40 56.5	9 25 15.9	0.93	0.4	<0.51		<30.23	4.6	99	
62*	6 40 56.7	9 37 49.1	1.09	0.4	0.77	0.3	30.39	9.0		W126(V88^m, S236^m, MX158, H41^m)
63*	6 40 56.7	9 30 09.2	1.02	0.3	1.02	0.3	30.38	5.5	90	W127(S235, F281^m, MX159)
64	6 40 58.2	9 30 53.8	3.97	1.2	<1.09		30.50	4.9		V93^m(S244^1, S245^{1,m}, F298, MX269, H43^m), S238(O102^m, F290, MX163)
65*	6 40 58.6	9 33 31.2	1.08	0.5	0.58	0.2	30.15	6.0		W132(V91^m, S242, F294, MX166)
66*	6 40 58.7	9 39 21.6	1.12	0.5	<0.45		<30.20	4.7	95	O103^m(MX168)
67*	6 40 58.7	9 53 48.4	87.35	3.2	77.19	5.8	32.30	106.8		V245^m
68*	6 40 59.1	9 55 24.2	2.05	0.7	1.81	0.5	30.63	6.8		V92^m(S249)
69*	6 40 59.2	9 53 06.6	1.20	0.4	0.86	0.3	30.31	6.1	99	S247
70*	6 40 59.3	9 46 19.1	0.91	0.4	0.69	0.3	30.25	7.1		S248^m, H44^m

Table 3. (continued)

N_X	RA_{2000} h m s	DEC_{2000} ^{o} ' "	$\mathrm{Rate_{max}}$ [c/ksec.]	err	$\mathrm{Rate_{min}}$ [c/ksec.]	err	$<\mathrm{Log(L_X)}>^a$ $[ergs\ s^{-1}]$	SNR	$\mathrm{P_{var}}$	Identifications
71*	6 40 59.5	9 35 11.8	1.63	0.6	0.84	0.3	30.39	6.3		W136(S251, O104^m, F305, MX173)
72*	6 40 59.6	9 51 51.4	0.87	0.4	0.87	0.4	30.31	4.8		S253(MX172)
73*	6 40 59.9	9 28 51.3	2.18	0.6	<1.24		30.71	7.1		F306^m(MX176)
74*	6 41 00.1	9 52 25.3	1.24	0.4	1.20	0.4	30.45	6.4		W137(V94^m, S254, MX175)
75*	6 41 00.3	9 29 10.4	3.47	0.9	1.90	0.6	30.92	7.0	99	S257(F309, MX179)
76*	6 41 00.4	9 45 04.3	0.60	0.2	<0.58		30.16	6.1		S258^m(O106^m, MX177)
77*	6 41 00.7	9 51 27.2	3.29	1.4	1.43	0.4	30.54	10.2		V96^m(S259, MX178)
78*	6 41 01.0	9 32 44.9	1.87	0.5	0.72	0.2	30.38	7.2	90	W139(V98, S260^m, F313, MX181, H47^m)
79	6 41 01.3	9 34 51.9	1.65	0.6	0.48	0.2	30.19	6.7	90	F314(S261^{1,m}, S262^{1,m}, O107^m)
80*	6 41 01.3	9 34 08.6	2.00	0.7	<0.77		30.36	7.3		V100(S263, F315, MX182)
81	6 41 01.6	9 48 25.8	3.53	0.5	1.67	0.6	30.87	17.8	99	V99^m(S265^1, S266^1, MX183)
82*	6 41 01.8	9 38 44.1	0.89	0.3	0.65	0.2	30.19	6.5		W146(V103^m, S267, MX186)
83	6 41 01.9	9 52 52.4	3.03	0.9	2.66	0.8	30.83	11.3		V101^m(S268^1,S269^1)
84*	6 41 02.2	9 51 59.1	1.51	0.6	1.41	0.4	30.52	9.1		V104^m(S270, MX187)
85*	6 41 02.4	9 34 57.7	8.72	1.0	1.26	0.4	30.98	19.7	99	W149(V105, S271, F321, MX189)
86*	6 41 02.5	9 35 14.1	0.87	0.3	0.69	0.2	30.22	6.7		W150(S272, F322)
87*	6 41 02.5	9 27 23.8	1.28	0.5	0.82	0.3	30.29	5.4		V108(F324, MX188)
88*	6 41 03.1	9 53 56.6	3.85	0.7	<1.65		30.59	10.9	99	
89*	6 41 03.4	9 31 19.4	4.71	0.8	2.01	0.6	30.95	16.8		V109^m(S279, F330, MX195)
90*	6 41 03.7	9 27 39.1	1.46	0.6	0.97	0.3	30.36	6.3		F335^m
91*	6 41 03.9	9 49 14.2	1.12	0.3	1.10	0.5	30.42	8.0	95	S281(MX196)
92	6 41 03.9	9 30 20.9	1.57	0.6	<0.53		<30.27	4.7	99	
93*	6 41 04.0	9 35 21.8	0.59	0.2	0.59	0.2	30.15	4.7		S282(F339)
94*	6 41 04.2	9 48 26.6	0.81	0.3	0.65	0.2	30.19	6.4		W156(V112^m, S285, MX198)
95	6 41 04.2	9 51 57.2	9.40	1.1	4.74	1.9	31.34	23.4	99	V110(S284, MX199), V111^m(S286)
96*	6 41 04.6	9 36 28.6	0.97	0.4	0.62	0.2	30.20	6.9		W159(V118^m, S290, F349, MX207)
97	6 41 04.8	9 53 19.1	1.27	0.4	1.25	0.4	30.47	6.6		S288, S295
98*	6 41 05.3	9 33 15.0	2.54	0.8	1.04	0.5	30.50	9.2		W160(S296, F351, MX213)
99	6 41 05.6	9 31 37.9	1.37	0.5	<0.71		30.22	5.3	95	F357, F352
100*	6 41 05.7	9 31 02.4	1.41	0.4	0.73	0.2	30.41	7.3		W162(S298, F353, MX215)
101*	6 41 06.0	9 36 25.3	4.82	1.3	1.41	0.4	30.84	15.2	99	W164(V122^m, S303^m, F360, MX219, H53^m)
102	6 41 06.1	9 54 21.7	2.51	0.8	<1.42		30.53	5.7	90	S297, O111^m
103*	6 41 06.3	9 29 33.9	3.86	1.2	<0.93		30.66	6.6		F361
104	6 41 06.7	9 27 33.6	5.66	0.8	2.03	0.8	31.03	14.4	99	V124^m(F367, MX225, H56^m), F371^1(H54^m)
105*	6 41 07.0	9 27 49.4	1.73	0.5	0.85	0.3	30.49	10.1	99	F370^m(MX227)
106*	6 41 07.1	9 25 53.8	1.45	0.6	0.88	0.3	30.32	6.9		O115^m(F374, MX229)
107*	6 41 07.3	9 31 22.1	1.39	0.5	<0.51		<30.24	5.4	99	F372
108*	6 41 07.7	9 44 04.9	1.24	0.2	0.92	0.3	30.47	9.0	90	W169(V126^m, S309, MX231)
109*	6 41 08.2	9 30 44.2	0.79	0.3	0.79	0.3	30.27	5.2		W175(S310, F378, MX233)
110*	6 41 08.5	9 42 54.1	0.78	0.3	0.74	0.2	30.25	7.2		W173(S312, MX236)
111*	6 41 08.8	9 23 42.1	5.67	1.0	2.27	0.8	30.90	16.0	95	F381(MX240)
112*	6 41 09.0	9 41 16.6	1.50	0.5	0.71	0.2	30.32	8.1	99	W174(V129, S315, MX238)
113*	6 41 09.6	9 28 01.1	1.28	0.6	<0.50		<30.26	4.8		V130
114*	6 41 09.7	9 27 12.1	2.76	0.8	2.41	0.8	30.77	14.2		V132(F385, MX245)
115*	6 41 10.0	9 27 47.7	4.82	0.9	3.74	0.5	30.95	17.7		V133(F386, MX247)
116*	6 41 11.9	9 26 29.2	0.56	0.2	0.56	0.2	30.12	4.9		W183(F398, H59^m)
117	6 41 12.6	9 52 44.1	3.57	1.0	2.39	0.7	30.81	10.2		W184(V137^m, S327^m, MX255, H60^m), S328(MX257)
118*	6 41 13.0	9 27 33.4	2.81	0.9	1.22	0.4	30.67	13.3		W189(V140^m, F401, MX262)
119*	6 41 13.0	9 23 04.2	0.52	0.2	0.52	0.2	30.09	4.8		MX263
120	6 41 13.2	9 26 12.7	4.68	0.7	3.50	1.1	31.05	15.6		V139^m(F406^1, F402^1, MX261^1, MX266^1, H62^m)
121*	6 41 13.2	9 13 49.6	1.97	0.8	<1.34		<30.59	4.9	90	
122	6 41 13.3	9 55 09.2	1.52	0.4	1.52	0.4	30.56	6.0		W186(S331^{1,m}, S332^1, MX258)
123*	6 41 13.4	9 24 37.1	1.66	0.7	<0.51		<30.28	4.5	99	MX264
124*	6 41 13.4	9 28 07.6	1.35	0.5	0.87	0.3	30.31	5.7		F404(MX268)
125*	6 41 14.4	9 37 14.1	9.60	0.9	0.60	0.2	30.95	21.8	99	
126*	6 41 14.6	9 33 25.6	1.20	0.4	0.65	0.3	30.39	6.3		W191(S335, F409, MX270)
127*	6 41 14.7	9 32 34.1	1.06	0.4	0.90	0.3	30.33	6.6		S336(F411, MX271)
128*	6 41 15.4	9 46 42.8	3.21	1.5	1.30	0.5	30.65	12.5		V143^m(S339, M367^m, MX274)
129	6 41 15.8	9 26 18.4	5.39	0.9	4.33	1.2	31.02	19.6	90	V147(F416, MX281)
130	6 41 16.3	9 26 33.4	0.94	0.5	<0.51		<30.24	4.7	95	
131*	6 41 16.4	9 29 51.4	3.21	1.3	<1.06		<30.58	4.7		V150(S343^m, M368^m, F418, MX285)
132*	6 41 16.6	9 36 18.9	0.60	0.3	<0.45		<30.10	4.7		F420(MX286)
133*	6 41 17.9	9 29 26.7	0.73	0.3	0.73	0.3	30.24	4.9		S346(F422, MX290)
134*	6 41 18.0	9 33 42.6	2.35	0.7	<0.85		30.30	6.5	99	W198(V152, S348, F424)
135*	6 41 18.3	9 33 51.5	8.58	1.0	1.00	0.4	30.93	19.2	99	W199(V153^m, S349^m, F426, MX295, H68^m)
136*	6 41 18.3	9 31 27.8	2.28	0.4	<1.45		30.54	11.4	99	F427(MX297)
137	6 41 18.5	9 39 44.1	0.59	0.2	0.51	0.2	30.08	5.3		S350^m(MX294, H67^m), S351(MX298)
138*	6 41 19.7	9 31 43.9	2.48	0.8	<1.23		30.60	12.1		V155^m(S353, F434, MX304)
139*	6 41 20.6	9 45 39.1	1.46	0.4	<1.01		30.54	9.7	95	V157^m(S355, MX306)
140*	6 41 20.7	9 47 34.2	0.60	0.2	0.60	0.2	30.15	4.8		MX305

Table 3. (continued)

N_X	RA_{2000} h m s	DEC_{2000} ^{o} ' "	$\mathrm{Rate_{max}}$ [c/ksec.]	err	$\mathrm{Rate_{min}}$ [c/ksec.]	err	$< \mathrm{Log(L_X)} >^a$ $[ergs\ s^{-1}]$	SNR	$\mathrm{P_{var}}$	Identifications
141*	6 41 21.0	9 33 37.8	2.61	0.9	0.76	0.3	30.40	8.1	90	W204(V159, S357^m, F440, MX308, H70^m)
142*	6 41 21.2	9 32 16.2	1.77	0.6	0.57	0.2	30.23	5.3	99	F441(MX309)
143*	6 41 21.7	9 45 34.1	0.78	0.3	0.54	0.2	30.11	5.5		V161(S359, MX310)
144*	6 41 22.0	9 43 14.9	1.11	0.4	0.76	0.3	30.28	7.4		S360(MX312)
145*	6 41 22.1	9 43 54.0	4.85	1.8	1.96	0.3	30.75	17.4	95	W206(V162^m, S362, MX313)
146*	6 41 23.1	9 27 25.9	4.48	0.8	3.04	0.9	30.93	18.1		W208(V164^m, F447, MX319)
147*	6 41 23.4	9 47 19.1	0.79	0.3	0.59	0.2	30.15	4.7		
148*	6 41 24.4	9 32 51.7	0.90	0.3	0.90	0.3	30.33	5.8		F452(MX324)
149	6 41 25.8	9 34 42.8	1.71	0.5	1.13	0.3	30.43	8.4	95	S370(F456, MX330) S372(F457)
150*	6 41 27.2	9 35 07.6	3.28	1.3	1.13	0.4	30.53	9.3		V170(S373, F460, MX335)
151*	6 41 27.3	9 51 19.2	0.79	0.3	0.79	0.3	30.27	4.6		W212(V168^m, S374^m)
152*	6 41 28.7	9 39 14.6	5.81	1.7	< 3.62		< 31.05	5.8		S382
153*	6 41 28.9	9 38 41.0	3.48	1.1	1.80	0.6	30.70	13.2		V173^m(S380)
154*	6 41 29.3	9 39 37.9	6.19	1.7	2.70	0.4	30.94	16.0		W214(V174^m, S381, MX339)
155*	6 41 31.6	9 48 36.5	1.60	0.6	1.36	0.4	30.51	8.9		V177(S388)
156*	6 41 32.4	9 38 09.1	2.39	0.8	< 0.77		30.54	6.1	95	V181^m(S394)
157*	6 41 32.9	9 19 02.5	1.68	0.6	< 0.97		30.36	6.3	90	W220(F473)
158*	6 41 37.3	9 45 11.5	1.54	0.5	< 0.89		30.33	6.5	99	V185(S407^m, H74^m)
159*	6 41 39.8	9 40 29.0	10.53	2.0	0.74	0.3	30.89	11.3	99	V191^m(S421^m, H77^m)
160	6 41 42.7	9 44 41.3	3.23	1.4	< 0.89		< 30.54	4.7		
161*	6 41 42.9	9 43 00.2	1.26	0.4	0.89	0.3	30.32	5.3		S433
162*	6 41 43.9	9 40 50.3	1.17	0.4	0.77	0.3	30.26	5.8		V200^m(S438^m, H79^m)
163*	6 41 45.3	9 44 44.1	1.00	0.3	1.00	0.3	30.37	5.6		S441
164*	6 41 45.4	9 47 13.9	1.28	0.4	0.90	0.3	30.33	5.3		
165	6 41 47.4	9 38 03.9	2.39	0.7	1.78	0.5	30.63	7.3		S446
166	6 41 48.1	9 42 44.5	9.19	2.8	2.03	0.6	30.92	15.7	95	V205^m(S450), S449
167	6 41 49.5	9 41 04.1	1.22	0.4	1.22	0.4	30.46	5.2		S454
168	6 41 50.3	9 29 51.4	6.01	1.5	< 3.99		31.14	6.7	99	S459, S465
169	6 41 55.0	9 30 14.0	1.56	0.5	1.56	0.5	30.57	5.7		S475, S478

[a] maximum likelihood X-ray luminosity - see text
* denotes unique counterparts - see text and plates
[1] part of a visual double system, unresolved by the other authors
[m] denotes that the counterpart is reported as a NGC 2264 member in the cited paper

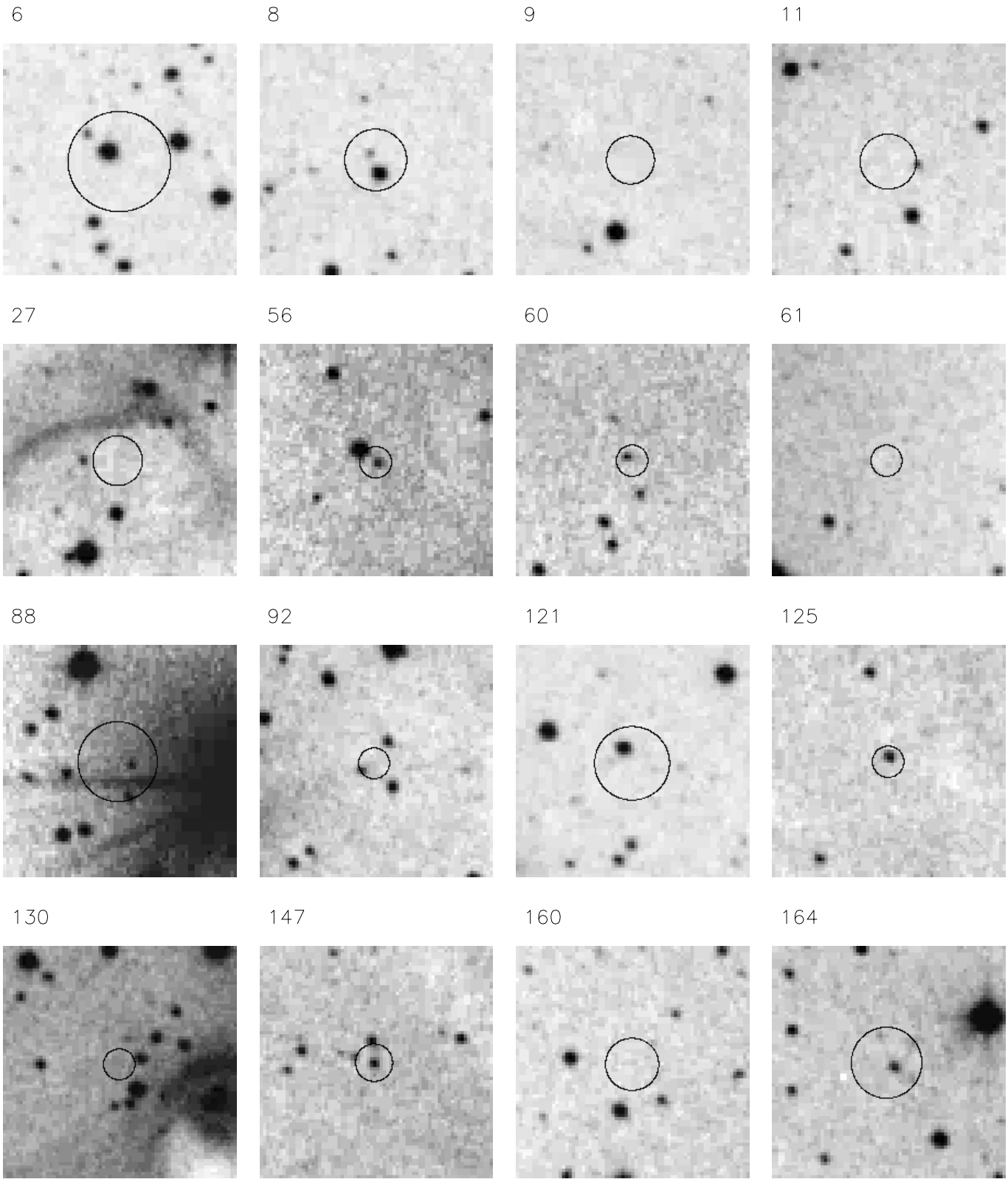

Fig. A.1. Finding charts for the sources with no cataloged counterpart